Frontal EEG-FNIRS Classification for Bipolar Disorder Diagnosis

Inès Tahir
CEA-Leti Minatec,
University of Grenoble Alpes,
Campus MINATEC,
F-38000, Grenoble, France
ines.tahir@cea.fr

Anne Planat-Chrétien
CEA-Leti Minatec,
University of Grenoble Alpes,
Campus MINATEC,
F-38000, Grenoble, France
anne.planat-chretien@cea.fr

Antoine Bertrand
CHU de Grenoble,
Service Hospitalo-Universitaire de Psychiatrie,
F-38000, Grenoble, France
abertrand4@chu-grenoble.fr

Mircea Polosan
University of Grenoble Alpes,
Inserm U1216, Grenoble Institut de Neurosciences,
CHU de Grenoble,
F-38000, Grenoble, France
MPolosan@chu-grenoble.fr

***Abstract*—Bipolar disorder is a mood disorder characterized by emotional and cognitive dysregulation, with often late diagnosis. This study explores a frontal system combining electroencephalography (EEG) and functional near-infrared spectroscopy (fNIRS) to aid diagnosis. The fNIRS system is confined to the frontal region to minimize interference from hair and EEG analysis is likewise restricted to this area. However, this restriction introduces ocular artifacts, traditionally removed using electrooculography. We propose an adaptive Artifact Subspace Reconstruction method—originally for high-amplitude noise correction—to address ocular artifacts without electrooculography, optimizing its parameters per subject and session. Specifically, we focus on the *k* parameter, which controls the artifact rejection threshold. Widely studied in literature, *k* influences signal correction and classification. We compared classification performance obtained using our adaptive *k* to that achieved with a fixed *k*, to evaluate the impact of each approach on signal correction and diagnostic accuracy. Given the spatial constraints of the setup, we combine EEG and fNIRS to enhance classification performance by exploiting their complementary properties and neurovascular coupling. Our results show that our frontal bimodal system, with adapted Artifact Subspace Reconstruction yields promising outcomes while preserving neural data integrity, demonstrating the feasibility of this approach for aiding bipolar disorder diagnosis.**

Keywords—Electroencephalography, Functional Near-Infrared Spectroscopy, Bipolar Disorder, Artifact Subspace Reconstruction, Adaptive Preprocessing

I. Introduction

Bipolar disorder (BD) is a mood disorder characterized by emotional and cognitive dysregulation. The emotional dysregulation manifests as deficits in the execution of cognitive tasks involving emotional interference. These deficits are tied to impaired fronto-limbic connectivity marked by hyperactivation of limbic areas and hypoactivation of frontal areas, as shown by neuroimaging studies particularly through the functional magnetic resonance imaging (fMRI) [1]. However, fMRI is costly, sensitive to movement artifacts and lacks portability, limiting its routine clinical use. In contrast, some studies have employed accessible techniques such as electroencephalography (EEG) and functional near-infrared spectroscopy (fNIRS). EEG records electrical activity, while fNIRS measures changes in oxygenated (HbO) and deoxygenated (HbR) hemoglobin concentrations in the brain. These modalities have been used to examine deficits in electrical activity [2] and perfusion [3] of BD patients. Studies combining the two modalities highlight impairments in fronto-limbic network [4] of BD patients.

Our study explores a combined frontal EEG-fNIRS setup for classification of BD patients (BP), healthy controls (HC) and BP subtypes (BPI and BPII). Although the system addressed the whole head for the EEG, had EOG electrodes, and optodes on the frontal part for the fNIRS, we focus only on the frontal part for both modalities. We hypothesize that this frontal setup could still reveal cortical markers of BD emotional dysregulation via an emotional Stroop task. The frontal area avoids some hair-related artifacts for the fNIRS, while it is more sensitive to ocular artifacts for the EEG, these ocular artifacts are typically corrected using an electrooculography (EOG)—a component excluded here to maintain a frontal system. To overcome this, we adapt the Artifact Subspace Reconstruction (ASR) method, traditionally used for high-amplitude artifact correction, to also eliminate ocular artifacts without EOG by optimizing its parameters per subject and session. Specifically, a critical component of ASR is the parameter *k*, which determines the threshold for artifact rejection. Previous studies have highlighted its influence on signal correction effectiveness [5] and classification outcomes [6]. Instead of using a fixed *k* parameter, we adapted *k* parameter per subject and session, to optimize artifact correction while maintaining signal integrity. Our approach aligns with the work of Kim et al. [7], who developed ASR variants to both enhance artifact removal and increase usable calibration data, thereby improving original ASR performance in challenging, real-world EEG signals. The reduced spatial coverage of EEG, may affect classification performances. fNIRS is added to compensate for this limitation as the combination of both methods exploits their complementary strengths (temporal and spatial resolution). It also enables addressing neurovascular coupling [8].

The study's objectives are: first to evaluate the feasibility of a frontal EEG-fNIRS system for classifying BD and its subtypes while addressing the challenges associated with a frontal setup (ocular artifacts). Second to assess the impact of our adapted ASR method, specifically by analyzing the impact of our adaptation of the *k* parameter compared to a fixed *k* on data correction, and classification accuracy.

We first address the challenge of limited EEG spatial coverage to the frontal region by adapting ASR to correct

ocular artifacts without EOG. Once the EEG and fNIRS signals are preprocessed, we apply a feature selection to reduce feature dimensionality, followed by a classification with a support vector machine (SVM). We compare results across different ASR strategies (adaptive *k* and fixed *k*) and modality combinations (EEG-only vs. EEG-fNIRS).

II. Materials and Methods

A. BipoNIRS clinical study

The study initially enrolled 25 HC and 46 BP, with 21 BPI and 25 BPII. Following the exclusion of data from participants with technical issues, the final cohort included 18 HC and 40 BP (19 BPI and 21 BPII).

The study performed a modified emotional Stroop task incorporating emotional images, based on the protocol established by Quan et al. [9]. The protocol design, illustrated in Fig. 1 comprises blocks of neutral, positive, and negative images and participants were instructed to identify the image frame color. The behavioral analysis on response data and response time of the BipoNIRS protocol is detailed in [10], revealing differential emotional interference processing in BD patients compared to HC.

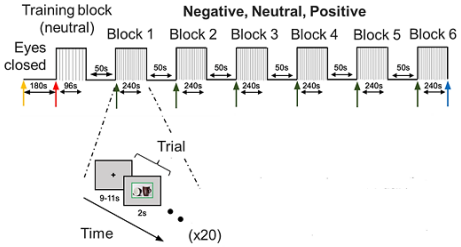

Fig. 1. BipoNIRS protocol presenting the experimental blocks (2 blocks of neutral, 2 blocks of negative, and 2 blocks of positive images) with inter-trial intervals (9-11s), rest periods (50s), and randomized order. It also indicates the resting phase at the beginning and the training phase with neutral images. Participants were instructed to respond "as quickly and as accurately as possible" to the color of the image frame, ignoring the emotional content, by pressing the corresponding keyboard key.

EEG data were collected with a 64-channel full-head EEG cap (10-20 system, ActiCap 64ch). To assess the feasibility of a frontal system, the analysis of EEG was restricted to the frontal part. fNIRS data were acquired using the OXYMON MK III system (Artinis), with 4 sources and 4 detectors, forming 6 channels on the prefrontal and frontal areas.

B. Preprocessing of EEG and fNIRS signals

The following pipeline is implemented within MATLAB toolboxes and EEGLab.

1) EEG

In standard EEG preprocessing pipeline, signals are first band-pass filtered [1-45] Hz and then ASR is applied to correct high-amplitude artifacts. ASR, introduced by T. Mullen and colleagues [11] is an effective Principal Component Analysis (PCA) based approach for EEG denoising. ASR is particularly advantageous because it reconstructs artifact-contaminated segments rather than eliminating them, preserving the integrity of the original data. In the literature, researchers apply ASR with default parameters. It is followed by Independent Component Analysis (ICA) to remove ocular component with a correlation between the Independent Component (IC) and the ocular signal recorded with the EOG. However, to develop a minimal frontal EEG-fNIRS system and get rid of EOG, we adapted the ASR method to correct ocular and motion artifacts. Our approach estimated ASR parameters dynamically based on the artifacts' distribution for each subject and session. The ASR depends on several predefined parameters, among which the cutoff *k* parameter is the most widely studied, as it determines the artifact rejection threshold. The parameter influences the proportion of data retained after signal correction by the ASR. In the literature, researchers typically set *k* based either on signal correction quality [5] or on classification outcomes [6]. Other ASR parameters are generally left at their default values, fixed to address high amplitude artifacts. However, in our study, we move beyond this fixed approach by implementing an adaptive method, enabling a more dynamic and subject and session specific correction strategy. To provide a clearer understanding of our adaptation, we recall its key steps in Equations (1) to (7), based on the original definition of ASR by Mullen et al. [11], and according to the notations we used in [5].

The ASR method comprises three main steps:

The first step consists of data calibration to determine clean segments $\mathbf{X}_0$ of EEG signals X. This calibration phase was performed on the beginning of the signal (0-300s) including a resting phase, and a short task execution period to ensure that both artifact-free and artifact-contaminated segments are present to get a relevant characterization of the artifacts.

In this calibration step, $\mathbf{X}$ is segmented using a sliding window of *windowlength* samples. To define *windowlength* parameter, we analyzed the artifact width distribution to size it according to the artifacts' duration. We wanted to get a broad understanding of artifact width in each channel. We began by detecting artifacts using the raw data distribution in each channel with the upper bound set at 98%. We chose this threshold to capture a subset of outliers sufficiently representative of ocular and movement artifacts to give a general idea of their widths in each channel without aiming for exhaustive detection. Fig.2 illustrates the frontal channel AF4 with small artifact widths due to ocular artifacts, which tend to be brief. Finally, the *windowlength* was determined as the maximum of the median artifact widths for each channel. The median was used to ensure that the estimated artifact widths reflect the general trend without the impact of extreme values. By taking the maximum of these medians across channels, we ensured that the selected window is sufficiently large to account for even the widest artifacts.

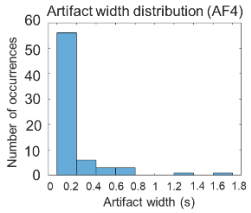

Fig. 2. Artifact width distribution for the frontal EEG channel AF4. The distribution shows ocular artifacts with small widths, which tend to be brief. Few larger artifacts are present corresponding to motion artifacts.

After segmenting $\mathbf{X}$ using a sliding window of size our estimated *windowlength*, the Root Mean Square (RMS) are computed and z-scored for each window and channel. A window is noted as *clean* if the z-scored RMS value for all channels belongs to the preliminary set data range *[ref1 ref2]*. The clean data $\mathbf{X}_0$ is obtained after rejecting all the data outside these bounds. To estimate references *[ref1 ref2]*, we analyzed the distribution of the z-scored RMS values

computed from the initial raw data. First, we identified outliers on each channel, corresponding to motion and ocular artifacts, ensuring that no artifacts were missed—particularly ocular artifacts, which are predominant in the frontal region (as illustrated in Fig. 3 on AF4, frontal). To establish the thresholds, we used the lower 5% and upper 95% bounds of the z-score distribution. Z-scores falling outside these bounds were classified as an artifact. Since the analysis was performed on multiple frontal EEG channels, each channel had its own lower and upper bounds values. To establish a representative global threshold that applies across all channels, we computed the mean of the z-scores at the lower and upper bounds across all channels, yielding the key reference values *[ref1 ref2]*.

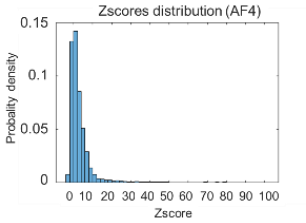

Fig. 3. Z-score distribution for the frontal EEG channel AF4. Most data points are low-amplitude fluctuations (neural activity), with low-amplitude outliers close to the mean, likely representing ocular artifacts. Additionally, few higher-amplitude artifacts are present, related to motion artifacts.

During the second step of the ASR, a rejection of artifacts threshold is defined based on these calibration data. The covariance matrix $\mathbf{C}_0$ of $\mathbf{X}_0$ is calculated. $\mathbf{C}_0$ is decomposed into its eigenvectors $\mathbf{U}_0$ and eigenvalues $\boldsymbol{\lambda}_0$ representing the principal components (PC) of the data (1).

$$\mathbf{C}_0 = \mathbf{C}_0 \mathrm{diag}(\boldsymbol{\lambda}_0)\mathbf{U}_0^T, \quad \mathbf{U}_0 = [\mathbf{u}_{0,1}, \ldots \mathbf{u}_{0,i}, \ldots \mathbf{u}_{0,Nc}] \quad (1)$$

Then the calibration data are transformed into the eigenvector space. It involves projecting the data onto the PC space. A PC score is computed as in (2).

$$\mathbf{y}_{0,i} = \mathbf{u}_{0,i}^T \mathbf{X}_0 \quad (2)$$

Once the PC scores are obtained, the data are segmented with a sliding window of *windowlength_calibrate* samples. We defined *windowlength_calibrate* equal to *windowlength*. For each window of each channel, the RMS is computed, as well as the mean $\mu_{0,i}$ and standard deviation $\sigma_{0,i}$. The rejection threshold for artifacts is defined on channel i by:

$$s_{0,i} = \mu_{0,i} + k \cdot \sigma_{0,i} \quad (3)$$

With k a unique cutoff parameter common to all channels representing the number of standard deviations $\sigma_{0,i}$ from the mean $\mu_{0,i}$, setting the artifact rejection threshold. We aimed to establish a stable and representative k parameter. Instead of using the z-score value at the upper bound 95% for each channel, the median across all channels was selected to define k parameter. This approach facilitates artifact identification while mitigating the impact of very high-amplitude artifacts, which could result in a k value that is not aggressive enough to correct ocular artifacts, and preventing overcorrection due to excessively low-amplitude artifacts. We compared our adaptive k with a fixed k value by evaluating both classification performance and percentage of retained data. This allowed us to determine which method better preserved the original signal, ensuring that the data used for classification remained representative and minimally affected by overcorrection. To define this fixed k parameter, we leveraged the distribution of adaptive k values observed across subjects in each group. The boxplots displayed in the Fig. 4 represent the adaptive k values for each subject per group. The fixed k was determined as the median of these subject-level k values within each group. This group-level median served as the fixed k value, ensuring a standardized correction threshold within each group.

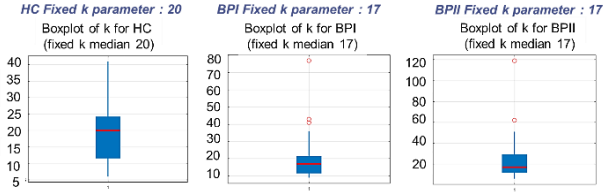

Fig. 4. Boxplots of k value for each subject within each group: patients with bipolar disorder type I (BPI), type II (BPII) and healthy controls (HC). Fixed k is defined as the median of adaptive k obtained per subject within each group (20 for HC, 17 for BPI and BPII).

Finally, the last step consists in segmenting the raw data $\mathbf{X}$ with a sliding window of *windowlength_recons* samples for each channel. We defined *windowlength_recons* equal to *windowlength*. As previously, the covariance matrix $\mathbf{C}$ is computed. It is decomposed into PC scores. Let us denote the $\mathbf{Y}$ the matrix of PC scores determined as:

$$\mathbf{Y} = \mathbf{U}^T \mathbf{X} \quad (4)$$

The eigenvalue of each score is compared to the rejection threshold $\mathbf{s}_0$ projected into this new space according to (5). It determines if the PC is clean or noisy for each channel.

$$\lambda_i < \|\boldsymbol{u}_i^T \mathbf{U}_0 \cdot \mathrm{diag}(\boldsymbol{s}_0)\|_2^2 \quad (5)$$

The ASR goal ASR is to correct artifacts without changing the signals' clean data. We denote the clean PC scores as:

$$\mathbf{Y}_A = \mathbf{U}_A^T \mathbf{X} \quad (6)$$

The idea is to find the solution $\hat{\mathbf{Z}}$ minimizing the Euclidean norm in the unconstrained least-squares problem defined as:

$$\Phi(\mathbf{Z}) = \left\| \mathbf{U}_A^T \mathbf{C}_0^{1/2} \mathbf{Z} - \mathbf{Y}_A \right\|_F^2 \quad (7)$$

With $\mathbf{Z}$, a zero-phase component analysis whitened EEG epoch. Finally, we obtain *clean* signals with the equation:

$$\mathbf{X}_{clean} = \mathbf{C}_0^{1/2} \hat{\mathbf{Z}} = \mathbf{C}_0^{1/2} \left(\mathbf{U}_A^T \mathbf{C}_O^{1/2} \right)^+ \mathbf{U}_A^T \mathbf{X} \quad (8)$$

2) fNIRS

fNIRS signals are impacted by various sources of noise categorized into physical artifacts and physiological artifacts (e.g., systemic intra- and extracerebral factors). To preprocess fNIRS data, we applied a band-pass filter [0.01-0.3] Hz, to remove physiological artifacts. Motion artifacts were corrected using Tukey's Biweight Robust Mean method and we utilized PCA [12] to mitigate the impact of extracerebral activities. This statistical method is used particularly when short-distance channel is unavailable.

C. Features selection and classification

To perform feature extraction, we epoched EEG signals into 2-second segments aligned with stimulus onset. We then computed event-related potentials (ERPs) for each condition and each subject on the frontal region. fNIRS signals were epoched on stimulus and post-stimulus resting periods to capture the full vascular response. We defined stimulus-evoked hemodynamic responses (SHRs) per subject by averaging HbO and HbR concentrations for each condition. Three time windows were defined on SHRs that focused on the signal delay (2-4s), the signal amplitude and slope (4-6s), the decline phase (6-8s). In parallel, we determined on ERPs time windows identified through statistical analysis and validated against literature [13] , [14]. These windows were

centered around peaks associated with specific cognitive processes: (70-130ms) a visual component, (200-300ms) an attention-related component, (450-650ms) an emotional one and (900-1100ms) related to a higher order cognitive function [13]. The integrals of ERPs/SHRs were calculated within these windows to construct the EEG and fNIRS feature sets. A feature selection was performed on fNIRS and EEG features independently to reduce dimensionality. It retained only the most relevant features, addressing the limited dataset size. A fusion approach was applied to combine the selected features of each modality into a unified vector, leveraging their complementary nature. We then employed an SVM classifier, optimizing its hyperparameters via grid search and 5-fold cross-validation on the training data, and then assessed its performance on independent test subject using leave-one-out cross-validation.

III. Results

Concerning the preprocessing of frontal EEG, a key challenge was the correction of ocular artifacts without EOG. Fig. 5 illustrates this correction with our adapted ASR on the frontal AF4 channel. The raw signal (blue) contains ocular artifacts and at the end of the signal, high-amplitudes (motion) artifacts are observed. The beginning of the signal (gray) represents the calibration phase for ASR parameters estimation with both artifact-free and artifact-contaminated segments. After applying ASR, the corrected signal (orange) shows a reduction in ocular artifacts and motion artifacts, while preserving the neural signal.

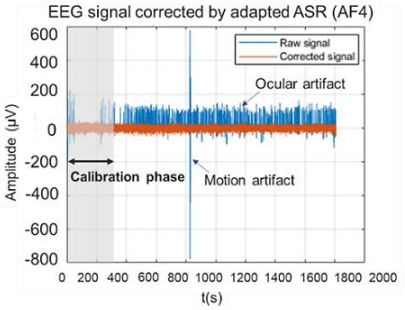

Fig. 5. Electroencephalography (EEG) signal correction using adapted Artifact Subspace Reconstruction (ASR) on AF4. The raw signal (blue) exhibits ocular artifacts and some motion artifacts. The signal beginning contains the calibration phase (gray area) for the ASR parameters estimation, with artifact-free and artifact-contaminated segments. After applying ASR, the corrected signal (orange) shows a correction of artifacts (ocular and high-amplitude), while preserving the neural activity (87% data retained).

To thoroughly assess the impact of the *k* parameter definition in the ASR, we compared classification results (EEG-only and EEG-fNIRS) using an adaptive *k* parameter versus a fixed *k* parameter. This comparative approach allows for a deeper understanding of how signal correction influences classification performance. Additionally, the classification enables us to assess whether the integration of fNIRS improves results, ensuring that we achieve acceptable performance with a frontal-only bimodal system.

BPI vs. HC classification (Fig. 6, a): For EEG-only classification, the adaptive *k* parameter achieved an accuracy of 84%, correctly identifying 83% of HC and 84% of BPI subjects. In contrast, the fixed *k* parameter resulted in a significantly lower accuracy of 68%. When integrating fNIRS, the accuracy remained at 81% with adaptive *k*. With fixed *k* it increased to 73%, reducing HC misclassification. However, while fNIRS improved classification with fixed *k*, the performance remained lower, especially for the classification of HC subjects than the adaptive *k* results.

BPII vs. HC classification (Fig. 6, b): For EEG-only classification, the adaptive *k* parameter achieved an accuracy of 67%, we observed a high misclassification rate for BPII (43%). With the fixed parameter, accuracy of 69% was slightly better, but with a high misclassification rate for HC (39%). When fNIRS was integrated, classification accuracy significantly increased to 82% with adaptive *k*, enhancing BPII classification (from 57% to 86%). With fixed *k*, the addition of fNIRS also improved BPII classification. However, HC classification remained lower (64%), suggesting that fixed *k* alters the balance of classification performance across groups.

BPI vs. BPII classification (Fig. 6, c): In the case of adaptive *k*, EEG-only identified 79% of BPI but with high misclassification rate for BPII (35%). Adding fNIRS further improved accuracy to 75%, particularly by reducing BPII misclassification (from 38% to 24%). With the fixed *k* parameter, EEG-only accuracy dropped to 62%, with high misclassification rates for both groups (37% for BPI, 38% for BPII). Although fNIRS integration slightly improved results, they remained significantly lower than those obtained with adaptive *k*. Results further confirmed that fixed *k* parameter alters the balance of classification performance across groups (no reduction in the misclassification rate for BPII).

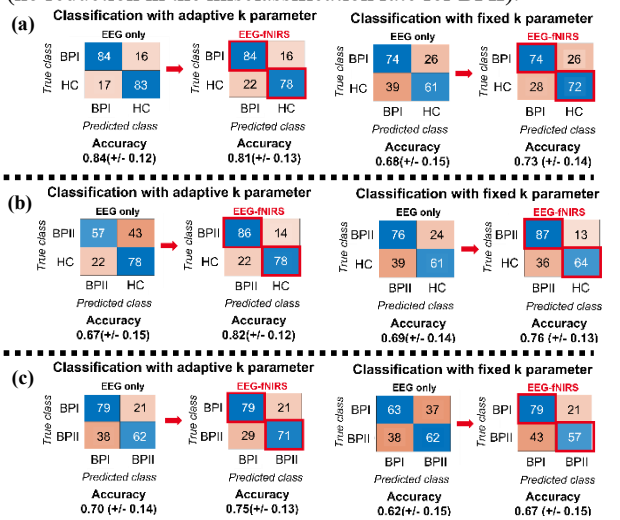

Fig. 6. Classification of groups – Patients with bipolar disorder type I (BPI), type II (BPII) and healthy controls (HC). Confusion matrices showing the classification performance with the adaptive *k* and the fixed *k* parameter : (a) BPI versus HC (b) BPII versus HC (c) BPI versus BPII. It compares the use of electroencephalography (EEG) alone (left) and combined with functional near infrared (fNIRS, right). The adaptive *k* approach outperformed fixed *k* in classification accuracy, with fewer misclassifications for HC subjects.

The results confirm the feasibility of a frontal EEG-fNIRS system for BD diagnosis. fNIRS integration enhances performance by reducing misclassification, especially for the classification of BPII subjects. However, careful attention must be paid to the definition of ASR parameters, which affect the correction of signals and classification accuracy. While some classifications (e.g., EEG-only BPII vs. HC) show better performance with a fixed *k* parameter, the boxplots Fig. 7 reveal a high dispersion in data retention compared to adaptive *k*. In particular, excessive correction was observed in some subjects BPI and BPII (up to 50% of data removed). This suggests that the filtering is too aggressive, correcting not only

noise but also potentially relevant signal information. Although fixed *k* occasionally yields better classification accuracy, it is crucial to question the quality of the data used for classification when signal is over-corrected. Higher classification accuracy with fixed *k* does not necessarily indicate better diagnostic validity, as it becomes unclear whether the model is distinguishing meaningful patterns or corrected segments. Unlike fixed *k*, the adaptive approach better preserves signal integrity by dynamically adjusting to each subject and session, ensuring that meaningful information is retained. It minimizes the risk of overcorrection, which could lead to misleading interpretations of classification results. This study highlights the importance of assessing the relevance of the *k* parameter not only in terms of classification performance but also in relation to the validity of processed data used for classification.

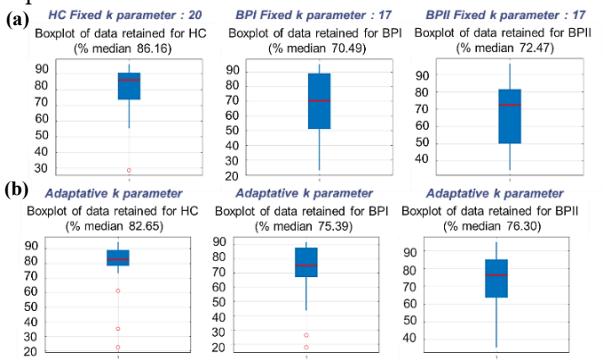

Fig. 7. Boxplot of the percentage of data retained for healthy controls (HC), patients with bipolar disorder type I (BPI) and type II (BPII) with adaptive *k* (a) versus fixed *k* (b). High dispersion in percentage of data retained with fixed *k*, with aggressive filtering in some BPI and BPII subjects (up to 50% data removal), potentially eliminating relevant information. With adaptive *k*, data dispersion is lower, ensuring better signal integrity preservation.

IV. Conclusion

This study demonstrates the feasibility of a frontal-only EEG-fNIRS system for BD diagnosis. Implementing an adaptive ASR parameter (*k*) for EOG-free artifact correction proved superior to a fixed-*k* strategy, effectively removing ocular artifacts while preserving true neural signals and enhancing classification reliability. Additionally, combining EEG with fNIRS mitigates frontal EEG's spatial limitations, notably improving bipolar II classification.

Limitations include a small sample size, age imbalance between BP and HC, and the use of PCA instead of the more effective short-distance channels for extracerebral contributions in fNIRS signals correction [15]. Future work will focus on validating the current findings on a larger dataset and by reserving a dedicated hold-out subset—or an entirely external dataset to better assess generalizability. Additionally, incorporating short-distance channels will be prioritized to enhance the accuracy of extracerebral signal correction.

Moreover, integrating a few strategically placed EEG electrodes beyond the frontal region could enhance system robustness while keeping a minimal setup. For real-world deployment, time efficiency, hardware costs, and user-friendliness will be crucial to ensure clinical applicability.

Acknowledgment

The database was developed on the IRMaGe platform with the assistance of Dr. A. Bertrand, M. Bouguerra, and E. Gil. The protocol was designed by Ronen Sosnik. The study received approval from the local ethics committee (CPP Sud-Est II - 2021-A00290-41).

References

[1] R. Mesbah, M. A. Koenders, N. J. A. van der Wee, E. J. Giltay, A. M. van Hemert, and M. de Leeuw, 'Association Between the Fronto-Limbic Network and Cognitive and Emotional Functioning in Individuals With Bipolar Disorder: A Systematic Review and Meta-analysis', *JAMA Psychiatry*, vol. 80, no. 5, pp. 432–440, May 2023, doi: 10.1001/jamapsychiatry.2023.0131.

[2] M. Carminati, F. Isel, J. Houenou, M. Wessa, and C. Henry, 'Impaired Regulation of Emotion in Bipolar I Disorder: Behavioral and Neurophysiological Signatures', *NeuroSci*, vol. 6, no. 1, Art. no. 1, Mar. 2025, doi: 10.3390/neurosci6010020.

[3] V. Quaresima and M. Ferrari, 'Functional Near-Infrared Spectroscopy (fNIRS) for Assessing Cerebral Cortex Function During Human Behavior in Natural/Social Situations: A Concise Review', *Organizational Research Methods*, vol. 22, no. 1, pp. 46–68, Jan. 2019, doi: 10.1177/1094428116658959.

[4] J. Kopf, 'Emotion processing and working memory deficits in Bipolar Disorder: interactions and changes from acute to remitted state', doctoralthesis, Universität Würzburg, 2018.

[5] N. Aloui, A. Planat-Chretien, and S. Bonnet, 'Artefact subspace reconstruction for both EEG and fNIRS co-registred signals', in *2021 43rd Annual International Conference of the IEEE Engineering in Medicine & Biology Society (EMBC)*, Mexico: IEEE, Nov. 2021, pp. 208–211. doi: 10.1109/EMBC46164.2021.9629641.

[6] C.-Y. Chang, S.-H. Hsu, L. Pion-Tonachini, and T.-P. Jung, 'Evaluation of Artifact Subspace Reconstruction for Automatic Artifact Components Removal in Multi-Channel EEG Recordings', *IEEE Trans Biomed Eng*, vol. 67, no. 4, pp. 1114–1121, Apr. 2020, doi: 10.1109/TBME.2019.2930186.

[7] H. Kim, C.-Y. Chang, C. Kothe, J. R. Iversen, and M. Miyakoshi, 'Juggler's ASR: Unpacking the principles of artifact subspace reconstruction for revision toward extreme MoBI', *Journal of Neuroscience Methods*, vol. 420, p. 110465, Aug. 2025, doi: 10.1016/j.jneumeth.2025.110465.

[8] R. Li, D. Yang, F. Fang, K.-S. Hong, A. L. Reiss, and Y. Zhang, 'Concurrent fNIRS and EEG for Brain Function Investigation: A Systematic, Methodology-Focused Review', *Sensors*, vol. 22, no. 15, Art. no. 15, Jan. 2022, doi: 10.3390/s22155865.

[9] S. Quan, Z. Wang, and Y. Liu, 'The Emotional Stroop Effect Is Modulated by the Biological Salience and Motivational Intensity Inherent in Stimuli', *Front. Psychol.*, vol. 10, p. 3023, Jan. 2020, doi: 10.3389/fpsyg.2019.03023.

[10] I. Tahir, A. Planat-Chretien, A. Pouchon, A. Bertrand and M. Polosan, 'Emotion regulation in bipolar disorder: A bimodal EEG-fNIRS study using an emotional Stroop task', *The Society for functional Near Infrared Spectroscopy*, Sept. 2024.

[11] T. Mullen *et al.*, 'Real-time modeling and 3D visualization of source dynamics and connectivity using wearable EEG', in *2013 35th Annual International Conference of the IEEE Engineering in Medicine and Biology Society (EMBC)*, Jul. 2013, pp. 2184–2187. doi: 10.1109/EMBC.2013.6609968.

[12] J. Virtanen, T. Noponen, and P. Meriläinen, 'Comparison of principal and independent component analysis in removing extracerebral interference from near-infrared spectroscopy signals', *J Biomed Opt*, vol. 14, no. 5, p. 054032, 2009, doi: 10.1117/1.3253323.

[13] K. K. Imbir *et al.*, 'Electrophysiological correlates of interference control in the modified emotional Stroop task with emotional stimuli differing in valence, arousal, and subjective significance', *PLoS One*, vol. 16, no. 10, p. e0258177, 2021, doi: 10.1371/journal.pone.0258177.

[14] L. M. Bylsma *et al.*, 'The late positive potential during affective picture processing: Associations with daily life emotional functioning among adolescents with anxiety disorders', *International Journal of Psychophysiology*, vol. 182, pp. 70–80, Dec. 2022, doi: 10.1016/j.ijpsycho.2022.09.009.

[15] S. Brigadoi and R. J. Cooper, 'How short is short? Optimum source-detector distance for short-separation channels in functional near-infrared spectroscopy', *Neurophotonics*, vol. 2, no. 2, p. 025005, Apr. 2015, doi: 10.1117/1.NPh.2.2.025005.